Author Manuscript

Author Manuscript

Author Manuscript

Author Manuscript

HHS Public Access

Author manuscript

Cytoskeleton (Hoboken). Author manuscript; available in PMC 2021 November 10.

Published in final edited form as:

Cytoskeleton (Hoboken). 2017 May ; 74(5): 205–218. doi:10.1002/cm.21364.

Re-evaluating the roles of myosin 18Aα and F-actin in determining Golgi morphology

Kyle Bruun[*], **Jordan R. Beach**[*], **Sarah M. Heissler**, **Kirsten Remmert**, **James R. Sellers**, **John A. Hammer**

Cell Biology and Physiology Center, National Heart Lung and Blood Institute, National Institutes of Health, Bethesda, MD 20892, USA

Abstract

The peri-centrosomal localization and morphology of the Golgi apparatus depends largely on the microtubule cytoskeleton and the microtubule motor protein dynein. Recent studies proposed that myosin 18Aα (M18Aα) also contributes to Golgi morphology by binding the Golgi protein GOLPH3 and walking along adjacent actin filaments to stretch the Golgi into its classic ribbon structure. Biochemical analyses have shown, however, that M18A is not an actin-activated ATPase and lacks motor activity. Our goal, therefore, was to define the precise molecular mechanism by which M18Aα determines Golgi morphology. We show that purified M18Aα remains inactive in the presence of GOLPH3, arguing against the Golgi-specific activation of the myosin. Using M18A-specific antibodies and expression of GFP-tagged M18Aα, we find no evidence that it localizes to the Golgi. Moreover, several cell lines with reduced or eliminated M18Aα expression exhibited normal Golgi morphology. Interestingly, actin filament disassembly resulted in a marked reduction in lateral stretching of the Golgi in both control and M18Aα-deficient cells. Importantly, this reduction was accompanied by an expansion of the Golgi in the vertical direction, vertical movement of the centrosome, and increases in the height of both the nucleus and the cell. Collectively, our data indicate that M18Aα does not localize to the Golgi or play a significant role in determining its morphology, and suggest that global F-actin disassembly alters Golgi morphology indirectly by altering cell shape.

Keywords

actin; Golgi; microtubule organizing center; myosin 18A

1 | INTRODUCTION

The Golgi apparatus is a peri-centrosomal organelle that functions as the main protein sorter within cells (Golgi, 1989; Palade, 1975). Following translation in the ER, proteins are conveyed through the Golgi, where they are post-translationally modified and sorted for

Correspondence: Jordan Beach, Cell Biology and Physiology Center, National Heart, Lung and Blood Institute, National Institutes of Health, Building 50, Room 2523, 9000 Rockville Pike, Bethesda, Maryland 20892., jbeach1@luc.edu.

[*]Kyle Bruun and Jordan R. Beach contributed equally to the work.

SUPPORTING INFORMATION

Additional Supporting Information may be found in the online version of this article.

Author Manuscript Author Manuscript Author Manuscript Author Manuscript

subsequent vesicular transport to various destinations (e.g., secretory vesicles, lysosomes, and the plasma membrane) (Palade, 1975). Structurally, the Golgi is composed of cisternae organized into ribbon-like stacks that closely associate with one another (Dalton & Felix, 1954). Each stack has a different chemical and enzymatic makeup, and as proteins move through them they are progressively modified in preparation for export (Glick & Luini, 2011, Kepes, Rambourg, & Satiat-Jeunemaitre, 2005). While the exact mechanism by which Golgi stacks cooperate to drive protein modification and sorting is still debated, there is general consensus that the overall function of the Golgi is dependent on its morphology (Glick & Luini, 2011).

The microtubule cytoskeleton plays a central role in determining the peri-centrosomal localization and morphology of the Golgi apparatus (Thyberg & Moskalewski, 1999). This is made possible by collaboration between the interphase microtubule array, which emanates from the centrosome and has its minus ends anchored there, and the microtubule minus end-directed motor dynein, which attaches to Golgi membranes (Yadav, Puthenveedu, & Linstedt, 2012). The net result of this collaboration is the maintenance of Golgi membranes near the centrosome. Consistently, both dynein inhibition and microtubule disassembly result in the rapid dispersion of Golgi cisternae throughout the cytoplasm (Harada et al., 1998; Minin, 1997). Interestingly, a second microtubule network that grows off Golgi membranes rather than the centrosome may also contribute to the maintenance of Golgi morphology (Miller et al., 2009; Sanders & Kaverina, 2015; Vinogradova et al., 2012; Zhu & Kaverina, 2013).

While microtubules and dynein clearly play a major role in determining Golgi distribution and organization, recent studies have also proposed roles for actin, actin-associated proteins, and myosin motors in regulating Golgi morphology and function. For example, some or all of these molecules have been implicated in the creation, scission, and transport of vesicles to, within, and away from the Golgi (Campellone, Webb, Znameroski, & Welch 2008; Cao et al., 2005; Carreno, Engqvist-Goldstein, Zhang, McDonald, & Drubin, 2004; Chen, Lacomis, Erdjument-Bromage, Tempst, & Stamnes, 2004; Coudrier & Almeida, 2011; Duran et al., 2003; Guet et al., 2014; Heimann, Percival, Weinberger, Gunning, & Stow, 1999; Jacob, Heine, Alfalah, & Naim, 2003; Kirkbride et al., 2012; Lazaro-Dieguez et al., 2007; Matas, Martinez-Menarguez, & Egea, 2004; Miserey-Lenkei et al., 2010; Stow, Fath, & Burgess, 1998). Most relevant to this study, alterations in Golgi morphology following actin filament disassembly have been reported (Dippold et al., 2009; Egea, Lazaro-Dieguez, & Vilella, 2006; Valderrama et al., 1998), leading to a model wherein actin filaments attached to the sides of Golgi cisternae extend them laterally to create the classic ribbon architecture (Dippold et al., 2009; Egea, Serra-Peinado, Salcedo-Sicilia, & Gutierrez-Martinez, 2013). Direct support for this model has been limited, however, as most studies employed global rather than Golgi-specific actin filament depletion, and the visualization of a Golgi-associated actin network capable of stretching the organelle has remained elusive. Recently, Field and coworkers (Dippold et al., 2009) appeared to provide strong support for this model by showing that myosin 18Aα (M18Aα), which resembles conventional type 2 myosin, binds to Golgi membranes, thereby identifying an actomyosin-dependent mechanism that in principal could establish and maintain Golgi morphology. Specifically, they presented evidence that M18Aα binds to the resident Golgi protein GOLPH3, possibly

Author Manuscript Author Manuscript Author Manuscript Author Manuscript

in a PDZ domain-dependent fashion (Taft et al., 2013), thereby allowing M18Aα to stretch the Golgi by walking along adjacent actin filaments (Dippold et al., 2009). Consistent with this idea, immunostaining suggested that endogenous M18Aα localizes to the Golgi, and the knockdown of either M18Aα or GOLPH3 caused Golgi ribbons to "collapse" into tight aggregates. Moreover, Golgi collapse was also observed following the addition of Latrunculin B to depolymerize cellular F-actin. Finally, Golgi collapse also occurred in cells expressing a mutated version of M18Aα predicted to lack motor function.

One significant concern with the model proposed by Field and coworkers is that M18Aα does not appear to be a functional motor. Specifically, the minimal ATPase activity exhibited by both vertebrate and *Drosophila melanogaster* M18A is not activated by F-actin, the common ATPase activator for the myosin family (Guzik-Lendrum, Nagy, Takagi, Houdusse, & Sellers, 2011; Guzik-Lendrum et al., 2013). Moreover, both are unable to translocate actin filaments in *in vitro* motility assays (Guzik-Lendrum et al., 2011, 2013). Consistent with these biochemical findings, M18A contains unusual substitutions at residue positions known to be required for myosin motor activity (Guzik-Lendrum et al., 2011, 2013; Heissler & Sellers, 2016). Given these observations, and the fact that mammalian M18A isoforms do not appear to assemble into bipolar filaments on their own (Billington et al., 2015), it seems highly unlikely that M18Aα could by itself remodel Golgi membranes by translocating them along actin filaments.

One way to reconcile the results of Field and coworkers (Dippold et al 2009) with the evidence that M18Aα is not a motor is the possibility that the myosin's ability to hydrolyze ATP and generate force requires another protein that was not included in previous ATPase assays. If GOLPH3 is one such protein, then M18Aα's mechanochemical activity might be locally activated at the Golgi. A second and perhaps more plausible way to reconcile these results revolves around the recent demonstration both *in vitro* and *in vivo* that M18Aα coassembles with conventional nonmuscle myosin 2 (NM2) to make heterotypic filaments (Billington et al., 2015). Specifically, by coassembling with NM2, M18Aα's inability to form filaments on its own or to translocate filaments no longer precludes its participation in events requiring force production. Given that M18Aα is present within cells at much lower levels than NM2 (~1 to 10, to 1 to 200) (Billington et al., 2015; Tan, Yong, Dong, Lim, & Leung, 2008), the assumption is that a subset of NM2 bipolar filaments are interfused with a few molecules of M18Aα. As for the functional role of the M18Aα molecules in these heterotypic filaments, the most obvious possibility is that they serve to connect the filaments to cellular structures, and/or to recruit molecules to the filaments, by virtue of the protein-protein interaction domains displayed at their N- and C-termini. One example of this could certainly be to recruit/connect heterotypic filaments to Golgi membranes via an interaction between M18Aα's PDZ domain and GOLPH3. In this scenario, therefore, M18Aα would still be required for normal Golgi morphology because it connects heterotypic filaments to Golgi membranes, although it would be the NM2 molecules within these mixed filaments that would be doing the mechanical work involved in stretching Golgi stacks.

The goal of this study was to reassess the role of M18Aα in determining Golgi morphology based on the information we now have regarding its biochemical properties and its ability to co-assemble with NM2. First, we found that GOLPH3 does not activate M18Aα's ATPase

Author Manuscript Author Manuscript Author Manuscript Author Manuscript

activity *in vitro*, arguing against the Golgi-specific activation of the myosin in cells. Most importantly, we found no evidence that M18Aα localizes to the Golgi, and we did not observe any significant defects in Golgi morphology in several cell lines that were either depleted of or devoid of M18Aα. We did, however, see a reduction in the lateral stretching of the Golgi following actin disassembly that mirrored the results of Field and coworkers (Dippold et al., 2009). Importantly, we found that this reduction in lateral stretching was accompanied by an expansion of the Golgi in the vertical direction, and that changes in the width and height of Golgi stacks following F-actin disassembly correlated with changes in the width and height of the nucleus, and with the height of the centrosome. These observations, together with additional data, indicate that M18Aα does not play a significant role in determining Golgi morphology, and suggest that the previously reported change in Golgi morphology seen following actin filament disassembly (Dippold et al., 2009; Egea et al., 2006, 2013; Valderrama et al., 1998) is a consequence of changes in cell shape, nuclear shape, and centrosome position.

2 | RESULTS

2.1 | M18Aα remains inactive in the presence of GOLPH3

The single *Myo18A* gene gives rise to at least two splice variants known as M18Aα and M18Aβ (Mori et al., 2003). M18Aα differs from M18Aβ in that it contains a 332-residue N-terminal extension that harbors the PDZ domain thought to be responsible for binding GOLPH3 (Taft et al., 2013) [Figure 1a]. As discussed in the introduction, previous work has shown that both M18Aα and M18Aβ lack F-actin-activated ATPase activity (Guzik-Lendrum et al., 2011, 2013) and are unable to translocate actin filaments in *in vitro* motility assays (Guzik-Lendrum et al., 2013). The possibility remains, however, that M18A requires a protein cofactor to exhibit significant ATPase activity. If GOLPH3 were to serve this purpose, then M18Aα's mechanochemical activity might be activated at the Golgi. To address this possibility, we measured the F-actin-activated ATPase activity of M18Aα in the presence and absence of GOLPH3. Figure 1b, shows that M18Aα exhibits essentially no actin-activated ATPase activity whether or not GOLPH3 is present (at a molar ratio of 1:4), while the positive control (NM2A) displays significant actin-activated ATPase activity. Although other binding partners might activate M18Aα's mechanochemical activity in cells, our data argue against a GOLPH3-dependent, Golgi-specific activation of M18Aα.

2.2 | M18Aα does not localize to the Golgi

To begin to test the hypothesis that M18Aα's role in stretching the Golgi (Dippold et al., 2009) is mediated through its ability to coassemble with NM2, we attempted to confirm the previously reported co-localization of endogenous M18Aα with Golgi stacks (Dippold et al., 2009) using two polyclonal antibodies against M18Aα. Antibody #1 was generated by immunizing a rabbit with a KLH-conjugated peptide corresponding to the C-terminal 18 residues of M18Aα, while Antibody #2 was raised by introducing into a rabbit a protein expression construct containing the C-terminal 100 residues of M18Aα (see Figure 1a). Both antibodies recognize M18Aα in western blots of whole cell extracts (Figure 1c). Of note, both antibodies also recognize M18Aβ (Figure 1c,d). As expected from previous work (Billington et al., 2015; Hsu, Tsai, Hsieh, Lyu, & Yu, 2010; Mori et al., 2005; Tan

Author Manuscript Author Manuscript Author Manuscript Author Manuscript

et al., 2008), both antibodies robustly label sub-nuclear actin stress fibers (Figure 2 a1–a3 and b1–b3; see inside dashed area) and actin-rich lamella (Figure 2 a1–a3 and b1–b3; see arrowheads) visible at the base of mouse embryo fibroblasts (MEFs). Antibody #1 did not, however, exhibit any obvious colocalization with the *cis*-Golgi marker GM130 in maximum intensity projections of MEFs (Figure 2 c1–c4). In contrast, Antibody #2 exhibited significant colocalization with Golgi membranes in MEFs (Figure 2 d1–d4; see red arrows), although this was not seen using other cell lines (data not shown). To resolve these discrepancies, we used CRISPR-mediated gene editing to create a MEF cell line devoid of both M18Aα and M18Aβ (M18A KO) (Figure 1d, lanes 1 and 2). While sub-nuclear and lamellar signals were completely absent when these M18A KO MEFs were immuno-stained with both antibodies (Figure 2 e1–e4 and f1–f4), the Golgi signal persisted with Antibody #2 (Figure 2f1–f4; see red arrows). The most straightforward interpretation of this result is that the Golgi signal observed with Antibody #2 is not due to M18Aα/M18Aβ but to cross-reaction with another protein that is present on the Golgi. Taken together, these results do not support the idea that endogenous M18Aα associates with Golgi membranes.

To confirm the antibody staining, we cotransfected HeLa cells with EGFP-tagged M18Aα and a Halo-tagged version of the cis-Golgi marker mannosidase II (Mann II-Halo). Z-stacks of cells collected with Zeiss Airyscan technology showed strong localization of EGFP-M18Aα at the base of the cell (Figure 3a1,a2), where it is known to colocalize with NM2 in ventral and sub-nuclear stress fibers (Billington et al., 2015; Hsu et al., 2010; Tan et al., 2008). As expected, these ventral sections contained little or no signal for the cis-Golgi (Figure 3 a6 and a7). In contrast, no obvious localization of EGFP-M18Aα was observed in planes further from the coverslip where the Golgi signal was prominent (Figure 3, compare Panels a3–a5 to Panels a8–a10; see also the merged images in Panels A11–A15). To exclude the possibility that this static imaging was missing transient localization of EGFP-M18Aα to the Golgi apparatus, we performed live-cell, time-lapse imaging in two different focal planes, one near the bottom of the cell where the EGFP-M18Aα signal was strong, and one near the middle of the cell where the Golgi signal was strong. In the lower plane, dynamic movements of EGFP-M18Aα were evident, consistent with its known targeting to ventral actomyosin structures (Figure 3 b1–b5; see also Video S1 in Supporting Information). In the upper plane, on the other hand, no transient localization of EGFP-M18Aα with the Golgi apparatus was observed (Figure 3 b6–b10; see also Video S1 in Supporting Information). We conclude, therefore, that neither endogenous M18Aα nor exogenously-expressed, EGFP-tagged M18Aα exhibit significant co-localization with the Golgi apparatus.

2.3 | Loss of M18Aα does not alter Golgi morphology or dynamics

While the localization data in Figures 2 and 3 are not consistent with a role for M18Aα in defining Golgi morphology (with or without NM2), the pool of M18Aα that regulates Golgi morphology could be very small and therefore difficult to detect with light microscopy. To test for this functional pool, we compared the morphology of the Golgi in control cells to cells in which the level of M18Aα was either greatly reduced using shRNA-mediated knockdown (M18A KD) in HeLa cells (Figure 1d, lanes 3–5) or eliminated using CRISPR-mediated gene editing (M18A KO) in MEFs (Figure 1d, lanes 1 and 2) and Rat2 fibroblasts (Figure 1d, lanes 6 and 7; see also Figure S1 in Supporting Information). In contrast to the

Author Manuscript Author Manuscript Author Manuscript Author Manuscript

study of Dippold et al., which showed that Golgi ribbons are almost always extended in control cells and collapsed in M18Aα knockdown cells (Dippold et al., 2009), we observed a wide range of Golgi morphologies in both control and M18A KD/KO cells. Specifically, all samples exhibited significant variation in Golgi morphology that ranged from very extended (i.e., where the Golgi was spread laterally around a significant fraction of the nucleus; see as examples Figure 4 a1 and b1) to quite contracted (see as examples Figure 4a2 and b2). To quantify the distributions of Golgi morphologies in control and M18A KD/KO cells, we imaged cells stained for GM130 and a nuclear dye using 3D microscopy (so as to collect the entire Golgi signal), created maximum intensity projections, and measured the fraction of nuclear perimeter occupied by the Golgi signal. This quantitation showed that neither the reduction (HeLa) nor abrogation (Rat2 and MEF) of M18Aα expression had any significant effect on Golgi morphology relative to control or wild-type (WT) cells (Figure 4c). Notably, this quantitation also confirmed the large variability in Golgi morphology, with the Golgi occupying between ~20% and ~80% of nuclear perimeter. Finally, images of the trans-Golgi network in control and M18A KD cells stained for VTi1A, 3D reconstructions of Golgi stacks in control and M18A KD cells stained for GM130, and measurement of the height of Golgi stacks in control and M18A KO cells, all support the conclusion that M18Aα is not required for normal Golgi morphology (Figure S2 in Supporting Information).

To continue efforts to identify a role for M18Aα in determining Golgi morphology and to further characterize the large degree of variability we observe in Golgi morphology, we turned to quantitative live-cell imaging. As described above, no specific Golgi morphology was ingrained for either WT or M18A KD/KO cells. Indeed, time-lapse imaging of individual cells expressing Mann II-mEmerald to mark the Golgi (and mCherry-H2B to mark the nucleus) showed that Golgi morphology continuously transitions between extended and collapsed morphologies over time (Video S2 in Supporting Information). To quantify the dynamics of these transitions, we measured the ratio of Golgi area to Golgi perimeter (A/P) over time (note that our use of the term dynamics here refers exclusively to large-scale changes in Golgi morphology and not to the dynamics of Golgi-derived vesicles). This metric yields a value of ~3 for a collapsed Golgi, and a value of ~1.5 for an extended Golgi (see the examples in Figure 4 d1–d6; the A/P values are indicated at the top right corner). Plots of A/P values for 15 HeLa cells expressing nontargeting shRNA (Figure 4e) and 15 HeLa cells expressing M18A shRNA (Figure 4f) over 12 hr (and determined every 10 minutes) showed that while the clear majority of NT HeLa and M18A KD HeLa cells exhibit frequent fluctuations in Golgi morphology, A/P values in both cases tended to fall between ~1.5 and ~3.0, with a mean of ~2.2. This conclusion was borne out by plotting the A/P values at every time point (Figure 4g), which yielded values for NT HeLa (2.20 ±0.42) and M18A KD HeLa (2.19 ±0.42) that were not significantly different. Moreover, plotting the summed changes in *A/P* values per cell over 12 hr (Figure 4h) yielded values for NT HeLa (11.53 ± 2.73) and M18A KD HeLa (11.10 ±4.02) that were not significantly different. Finally, plotting the rates of change in *A/P* values per 10-min interval per cell going from either collapsed to extended and or from extended to collapsed (Figure 4i) yielded values for NT HeLa and M18A KD HeLa that were not significantly different. Together, these results argue that the Golgi apparatus is a highly dynamic organelle whose

Author Manuscript Author Manuscript Author Manuscript Author Manuscript

large-scale morphology does not depend in any significant way on the presence of M18Aα. We cannot exclude the possibility, however, that M18Aα is playing a role in the nanoscale architecture of the Golgi, or in the tubulation of Golgi membranes.

2.4 | Changes in Golgi morphology induced by actin filament disassembly correlate with changes in nuclear shape, centrosome position, and cell shape

We next sought to clarify the role played by the actin cytoskeleton in determining Golgi morphology, as numerous studies, including that of Dippold et al., have reported that disassembling actin filaments results in Golgi collapse (Dippold et al., 2009; Egea et al., 2006; Valderrama et al., 1998), and that this collapse is independent of changes in cell morphology (Valderrama et al., 1998). To accomplish this, we imaged Rat2 fibroblasts expressing mCherry-H2B to mark the nucleus and Mann II-mEmerald to mark the Golgi before and 15 min after the addition of 2 μM Latrunculin A (Lat A), which drives robust actin filament disassembly by sequestering actin monomers. Consistent with previous findings, we observed a significant reduction over time in the lateral extension of the Golgi following Lat A addition (see Figure 5 a1–a7, which show a maximum z-projection in an overhead view, and Figure 5 b1–b7, which show these same images following 3D-surface rendering; see also Video S3 in Supporting Information). This change was borne out quantitatively by measuring the fraction of nuclear perimeter occupied by the Golgi (Figure 4d; compare WT to WT+ Lat A for Rat2). Lat A treatment also caused Golgi “collapse” in HeLa cells expressing non-targeting shRNA (Figure 4d; compare NT to NT+ Lat A for HeLa), in HeLa cells expressing M18Aα shRNA (Figure 4d; compare M18A KD to M18A KD+ Lat A for HeLa), and in M18Aα KO Rat2 cells (Figure 4d; compare M18A KO to M18A KO+ Lat A for Rat2). Together, these results argue that actin filaments play an M18Aα-independent role in determining Golgi morphology.

The decrease in the lateral extension of the Golgi following actin filament disassembly could be due to the Golgi simply assuming a more compact morphology, that is, to Golgi collapse. Alternatively, this decrease might be accompanied by an expansion of the Golgi in the z dimension so as to balance the reduction in its xy dimensions. To begin to distinguish between these two possibilities, we viewed 3D-rendered cells from an orthogonal view (see Figure 5 c1–c7, which show the cell depicted in Panels B1-B7 from an orthogonal view; see also Video S3 in Supporting Information). This revealed that the Lat A-induced reduction in lateral extension of the Golgi seen in the surface-rendered overhead view (Figure 4 b1–b7) is accompanied by an expansion of the Golgi in the z dimension, that is, in the height of the Golgi (Figure 4 c1–c7). Importantly, the shape of the nucleus changed in a similar manner following Lat A treatment, with its width decreasing and its height increasing (Figure 4 c1–c7). Consistently, quantification demonstrated a strong positive correlation between nuclear height and Golgi height (Figure 5e), and between nuclear width and Golgi width (Figure 5f), following both Lat A treatment (grey section) and Lat A washout (white section) (see legend for statistics). This correlation between nuclear and Golgi height was not limited to their changes during F-actin disassembly, as stochastic variations in Golgi height correlated strongly with variations in nuclear height in both WT and M18A KO cells in steadystate conditions (Figure 4g). Together, these observations argue that the Golgi does not “collapse” following actin filament disassembly (Dippold et al., 2009; Egea et al., 2006, 2013), but

Author Manuscript Author Manuscript Author Manuscript Author Manuscript

rather undergoes a reconfiguring of its dimensions, and that the nucleus undergoes a similar reconfiguration.

Given the central role played by the microtubule cytoskeleton in determining Golgi localization and morphology, we asked if the centrosome/MTOC moves in a similar manner to the nucleus and Golgi upon actin filament disassembly. To do this, we expressed GFP-tubulin to indirectly mark the position of the MTOC (the site where microtubule minus ends converge) and Mann II-mCherry to mark the Golgi in Rat2 fibroblasts and performed 4D imaging during Lat A treatment and washout (Figure 6 a1–a4 and a5–a7, respectively see also Video S4 in Supporting Information). Orthogonal views created from z-stacks over time demonstrated that the MTOC does indeed move upward during Lat A treatment (Figure 6 b1–b4; the bright GFP-tubulin spot marked by the red arrow indicates the MTOC) and begins to move downward during washout (Figure 6 b5–b7). Moreover, the Golgi remains associated with the MTOC as it rises during Lat A treatment and falls during Lat A washout (Figure 6 c1–c4 and c5–c7, respectively). Indeed, MTOC movement corresponded strongly with Golgi movement throughout this process (Figure 6 d1–d7; see also Video S4 in Supporting Information), suggesting that changes in MTOC position are at least partially responsible for changes in Golgi morphology seen upon actin filament disassembly.

Finally, in addition to identifying the MTOC, GFP-tubulin provided a cytoplasmic marker to visualize overall cell shape (Figure 6). Importantly, this signal revealed a dramatic increase in the height of cells following Lat A treatment (Figure 6 b1–b4) that was partially reversed 20 minutes after washout (Figure 6 b5–b7). These observations are completely consistent with the central role played by the actin cytoskeleton in maintaining a flattened cell morphology in 2D cell culture by driving cell spreading and focal adhesion assembly (Kim, et al., 2012; Vishavkarma et al., 2014). Moreover, studies have shown that the transition from flat to round cell morphology following actin disassembly reduces the confinement of the nucleus, causing it to increase in height and decrease in width (Hatch & Hetzer, 2016; Vishavkarma et al., 2014). We conclude, therefore, that the alteration in Golgi morphology seen following actin filament disassembly is probably an indirect consequence of a large-scale change in cell shape, nuclear shape and MTOC position.

3 | DISCUSSION

At the outset of this work, we first expected to reproduce the results of Field and coworkers (Dippold et al., 2009) regarding M18Aα's requirement for creating the ribbon-like shape of the Golgi, and then to test an alternative model that includes a role for NM2 in this process, based on our recent demonstration that M18Aα coassembles with NM2 (Billington et al., 2015). Unfortunately, we found no evidence that M18Aα localizes to the Golgi or influences its organization in any significant way. Considering the *Myo18A* gene is spliced to create the two known isoforms, it remains possible that additional, unknown splice variants are expressed and contribute to Golgi morphology. What is clear from our localization and knockdown/knockout studies, however, is that M18Aα is not involved in determining overall Golgi morphology.

Author Manuscript Author Manuscript Author Manuscript Author Manuscript

Like previous studies (Dippold et al., 2009; Egea et al., 2006, 2013; Valderrama et al., 1998), we found that global actin filament disassembly causes a reduction in the lateral extension of the Golgi. Two models could explain this result. As previously suggested, an actomyosin network could directly engage Golgi stacks to stretch them laterally (Dippold et al., 2009; Egea et al., 2006, 2013; Valderrama et al., 1998). Alternatively, actin might mediate Golgi morphology indirectly by maintaining a flattened cell shape. For multiple reasons, we support the latter model. First, there is a lack of evidence, especially microscopy-based evidence, for an actomyosin network that could support the lateral stretching of the Golgi. Second, the actin cytoskeleton is known to play a central role in maintaining a flattened cell shape in 2D culture, and global actin filament disassembly typically results in both nuclear and cell rounding (Hatch & Hetzer, 2016; Khatau et al., 2009; Vishavkarma et al., 2014). Third, our data show that the reduction in lateral extension of the Golgi seen upon Lat A treatment is accompanied by axial expansion, and that this axial movement correlates strongly with increases in the heights of the MTOC, nucleus, and cell (i.e., with cell rounding). While this evidence is correlative in nature, we think the most reasonable interpretation of our data is that cell rounding induced by global actin filament disassembly is responsible for a reconfiguration of the Golgi that was previously misinterpreted as Golgi “collapse.” Importantly, we cannot exclude the possibility that F-actin does have a direct role in maintaining large-scale Golgi morphology. That said, arguments supporting such a role will require the identification and targeted disruption of actin networks that specifically associate with the Golgi, as assays involving global actin filament disassembly result in large changes in cell shape that preclude mechanistic insight. Finally, our conclusions do not preclude important roles for actin in Golgi processes like membrane tubulation and vesicle transport for which there is ample scientific support (Campellone et al., 2008; Cao et al., 2005; Carreno et al., 2004; Chen et al., 2004; Coudrier & Almeida, 2011; Duran et al., 2003; Guet et al., 2014; Heimann et al., 1999; Jacob et al., 2003; Kirkbride et al., 2012; Lazaro-Dieguez et al., 2007; Matas et al., 2004; Miserey-Lenkei et al., 2010; Stow et al., 1998).

4 | METHODS

4.1 | Cell culture and transfection

Cells were grown in Dulbecco’s modified Eagle’s medium supplemented with 10% fetal bovine serum, 2 mM GlutaMAX (Life Technologies, Grand Island, NY), and 1X antibiotic-antimycotic (Life Technologies), and maintained at 37°C in 5% CO_2. All coverslips were coated with 10 mg mL^{-1} fibronectin (Sigma, St. Louis, MO) prior to use. Cells were transferred to Leibovitz’s L-15 medium supplemented with 10% fetal bovine serum during live-cell imaging. Cells were transfected using a Lonza Nucleofector system in a solution containing 5 mM KCl, 15 mM $MgCl_2$, 120 mM Na_2HPO_4/NaH_2PO_4 (pH 7.2), and 50 mM mannitol, and using program I-13 for HeLa and program O-17 for Rat2.

4.2 | Antibodies and immunofluorescence

Cells were fixed in a solution containing 4% formaldehyde, 150 mM NaCl, 5 mM EGTA, 5 mM glucose, 5 mM $MgCl_2$, and 10 mM PIPES (pH 6.8). Cells were then simultaneously permeabilized and blocked in 1xPBS containing 0.2% Saponin and 5% normal goat serum.

Author Manuscript Author Manuscript Author Manuscript Author Manuscript

Primary and secondary antibody incubations were performed for 2 hr at room temperature in permeabilization/blocking solution. The mouse monoclonal antibody to GM130 was purchased from BD Transduction Laboratories (# 610822). Generation of the two rabbit polyclonal antibodies against myosin 18A was described previously (Billington et al., 2015). AlexaFluor-conjugated secondary antibodies and phalloidin were purchased from Life Technologies. Nuclear staining was performed using DAPI.

4.3 | Expression vectors

Plasmids Mann II-mEmerald, pmCherry-H2B and Mann II-pmCherry were gifts from Michelle Baird (Waterman Lab, CBPC, NHLBI, NIH). Plasmid Mann II-Halo was created by swapping the mEmerald fluorophore with the Halo tag using Age1 and BsrG1 restriction sites. Plasmid L304-EGFP-Tubulin-WT was a gift from Weiping Han (Addgene plasmid # 64060).

4.4 | Knockdown and knockout cell lines

For knockdown of M18A in HeLa, the cells were transduced with either non-targeting control shRNA (Sigma-Aldrich #SHC002) or M18A shRNA (TRCN0000107201: target sequence 5′-CCTCTTTGTCTCAGC GTGTTA-3′). Stable cell lines were established in 3 μg mL^{-1} puromycin. For knockout of M18A in MEFs and Rat2 cells, CRISPR/Cas9 technology was used (Ran et al., 2013). Primers were integrated into pSpCas9 (BB)-2A-Puro (PX459), which was a gift from Feng Zhang (Addgene plasmid # 48139). The Rat2 target sequence was 5′-AGGAGCTCAG CCTACCCGA-3′ and the MEF target sequence was 5′-GCAGGACGC TAGACTCGTTG-3′. M18A KO clones were isolated by single cell sorting into 96-well plates, followed by screening for M18A KO using Western blots of whole cell extracts.

4.5 | Imaging

Confocal imaging was performed on a Nikon A1R microscope equipped with a 40× 1.3 NA objective. Overnight imaging was performed on this microscope using a 20x air objective. Wide-field 3D imaging of fixed cells was performed on a DeltaVision OMX 3D-SIM Imaging System V4 (GE) equipped with an Olympus 60×/1.42 NA objective. Raw images were deconvolved using Softworx (Applied Precision). Wide-field imaging of the Golgi and nucleus in live cells was performed using Essen Biosciences Incucyte technology, which enables imaging inside of an incubator with a 20× objective. Zeiss Airyscan imaging was performed in either Fast Optimum mode (Figure 5 and Supporting Information Video S3) or in Super-resolution (SR) mode (Figures 3 and 6 and Supporting Information Videos S1 and S4) on a Zeiss LSM 880 Airyscan microscope equipped with a 63×/1.4 NA objective. Raw data was processed using Airyscan processing in “auto strength” mode with Zen Black software version 2.3. Linear adjustments for contrast and brightness were made to images using ImageJ.

4.6 | Protein production and actin-activated ATPase assay

FLAG-tagged mouse Halo-M18Aα and human NM2A heavy meromyosin were expressed in baculovirus/Sf9 insect cells, purified via FLAG-capture, and concentrated via

Author Manuscript Author Manuscript Author Manuscript Author Manuscript

ultrafiltration as described (Guzik-Lendrum et al., 2013; Kengyel, Wolf, Chisholm, & Sellers, 2010; Wang et al., 2003). Human GOLPH3-His_6 was obtained from Proteintech. F-actin was prepared from rabbit skeletal muscle acetone powder (Pel-Freez Biologicals) (PMID 4622352). ATPase assays was performed at an F-actin concentration of 40 μM with 0.15 μM NM2A or 0.12 μM M18A and 0.6 μM GOLPH3 in buffer containing 10 mM MOPS (pH 7.0), 2 mM $MgCl_2$, 0.15 mM EGTA, 40 U mL^{-1} *l*-lactic dehydrogenase, 200 U mL^{-1} pyruvate kinase, 200 μM NADH, 1 mM phosphoenolpyruvate, 50 mM NaCl, and 2 mM ATP at a temperature of 25°C for M18A and 35°C for NM2A as described (Guzik-Lendrum et al., 2013; Kengyel et al., 2010; Wang et al., 2003). NM2A was phosphorylated with myosin light chain kinase prior to the assay (PMID 20711642). The data were corrected for the background ATPase activity of F-actin (+/− GOLPH3) in the assay.

4.7 | Fraction of nuclear perimeter

Cells were imaged in wide-field 3D and processed as described above. A mask of the nucleus was then created from maximum intensity projections using the threshold tool in ImageJ. To avoid artefacts from differences in the contour of nuclei, which can dramatically influence the measured perimeter, we first smoothed the nuclear outline with 15-pixel interpolation. We then measured the nuclear perimeter and manually traced the nuclear perimeter over which the Golgi extended. The nuclear perimeter over which the Golgi extends divided by the total nuclear perimeter provided the fraction of nuclear perimeter measurement (Figure 4C,D). Data was graphed using Graphpad Prism. Statistical significance was determined using an unpaired *t* test with Welch's correction.

4.8 | Measuring Golgi dynamics

HeLa NT and HeLa M18A KD cells expressing mCherry-H2B and Mann II-mEmerald were imaged simultaneously every 10 minutes over a period of 12 hr on the Nikon A1R microscope using a 20× air objective. A mask of the Golgi was created for 30 randomly chosen cells (15 HeLa NT and 15 HeLa M18A KD) using the ImageJ threshold tool. The area and perimeter were measured at each point and the area divided by the perimeter was graphed using Graphpad Prism.

4.9 | Imaris 3D reconstruction

Z-stacks of Rat2 cells expressing mCherry-H2B and Mann II-mEmerald treated with 2 μM Lat A were acquired with Zeiss Airyscan imaging every 10 s with 0.5 μm steps, imported into Imaris 3D visualization software (Bitplane), and the different channels analyzed. The 3D rendering of each channel was performed using the "Surfaces" tool in Imaris software.

4.10 | Nuclear and Golgi height measurements

For fixed-cell experiments (Figure 5G), Rat2 cells were stained and imaged as in the nuclear perimeter experiments (see above). For live-cell experiments (Figure 5E,F), Rat2 cells expressing mCherry-H2B and Mann II-mEmerald were acquired with Zeiss Airyscan imaging every 30 s in 0.5 μm steps. The cells were imaged for 3 min, subjected to 2 μM Lat A for 10 min, and then imaged for 10 min after Lat A washout. In ImageJ, images were rotated so that the maximum width of the Golgi was oriented parallel to the image border.

Author Manuscript Author Manuscript Author Manuscript Author Manuscript

The z-stack was then “resliced” from the direction of that border, and a maximum projection of this new stack was created. Next, the threshold tool was used to create a mask of both the Golgi and the nucleus and a “bounding box” was created for each organelle to measure the height and, where indicated, the width. For live-cell imaging, this analysis was performed at each time point. All statistics were plotted in Graphpad Prism. Pearson’s correlation was used to determine R^2 values and statistical significance.

Supplementary Material

Refer to Web version on PubMed Central for supplementary material.

ACKNOWLEDGMENTS

The authors thank Sricharan Murugesan (NHLBI) and Xufeng Wu (NHLBI Light Microscopy Core) for help with imaging, Zac Swider (NHLBI) for helpful suggestions with analysis, and Luke Lavis (Janelia Research Campus) and Julie Donaldson (NHLBI) for reagents.

REFERENCES

Billington N, Beach JR, Heissler SM, Remmert K, Guzik-Lendrum S, Nagy A, … Sellers JR (2015). Myosin 18A coassembles with nonmuscle myosin 2 to form mixed bipolar filaments. Current Biology, 25, 942–948. [PubMed: 25754640]

Campellone KG, Webb NJ, Znameroski EA, & Welch MD (2008). WHAMM is an Arp2/3 complex activator that binds microtubules and functions in ER to Golgi transport. Cell, 134, 148–161. [PubMed: 18614018]

Cao H, Weller S, Orth JD, Chen J, Huang B, Chen JL, … McNiven MA (2005). Actin and Arf1-dependent recruitment of a cortactin-dynamin complex to the Golgi regulates post-Golgi transport. Nature Cell Biology, 7, 483–492. [PubMed: 15821732]

Carreno S, Engqvist-Goldstein AE, Zhang CX, McDonald KL, & Drubin DG (2004). Actin dynamics coupled to clathrin-coated vesicle formation at the trans-Golgi network. Journal of Cell Biology, 165, 781–788.

Chen JL, Lacomis L, Erdjument-Bromage H, Tempst P, & Stamnes M (2004). Cytosol-derived proteins are sufficient for Arp2/3 recruitment and ARF/coatomer-dependent actin polymerization on Golgi membranes. FEBS Letters, 566, 281–286. [PubMed: 15147909]

Coudrier E & Almeida CG (2011). Myosin 1 controls membrane shape by coupling F-Actin to membrane. Bioarchitecture, 1, 230–235. [PubMed: 22754614]

Dalton AJ & Felix MD (1954). Cytologic and cytochemical characteristics of the Golgi substance of epithelial cells of the epididymis in situ, in homogenates and after isolation. American Journal of Anatomy, 94, 171–207.

Dippold HC, Ng MM, Farber-Katz SE, Lee SK, Kerr ML, Peterman MC, … Field SJ (2009). GOLPH3 bridges phosphatidylinositol-4- phosphate and actomyosin to stretch and shape the Golgi to promote budding. Cell, 139, 337–351. [PubMed: 19837035]

Duran JM, Valderrama F, Castel S, Magdalena J, Tomas M, Hosoya H, … Egea G (2003). Myosin motors and not actin comets are mediators of the actin-based Golgi-to-endoplasmic reticulum protein transport. Molecular Biology of the Cell, 14, 445–459. [PubMed: 12589046]

Egea G, Lazaro-Dieguez F, & Vilella M (2006). Actin dynamics at the Golgi complex in mammalian cells. Current Opinion in Cell Biology, 18, 168–178. [PubMed: 16488588]

Egea G, Serra-Peinado C, Salcedo-Sicilia L, & Gutierrez-Martinez E (2013). Actin acting at the Golgi. Histochemical Cell Biology, 140, 347–360.

Glick BS & Luini A (2011). Models for Golgi traffic: A critical assessment. Cold Spring Harbor Perspectives in Biology, 3, a005215. [PubMed: 21875986]

Golgi C (1989). On the structure of nerve cells. 1898. Journal of Microscopy, 155, 3–7. [PubMed: 2671382]

Author Manuscript Author Manuscript Author Manuscript Author Manuscript

Guet D, Mandal K, Pinot M, Hoffmann J, Abidine Y, Sigaut W, … Manneville JB (2014). Mechanical role of actin dynamics in the rheology of the Golgi complex and in Golgi-associated trafficking events. Current Biology, 24, 1700–1711. [PubMed: 25042587]

Guzik-Lendrum S, Heissler SM, Billington N, Takagi Y, Yang Y, Knight PJ, … Sellers JR (2013). Mammalian myosin-18A, a highly divergent myosin. Journal of Biological Chemistry, 288, 9532–9548.

Guzik-Lendrum S, Nagy A, Takagi Y, Houdusse A, & Sellers JR (2011). Drosophila melanogaster myosin-18 represents a highly divergent motor with actin tethering properties. Journal of Biological Chemistry, 286, 21755–21766.

Harada A, Takei Y, Kanai Y, Tanaka Y, Nonaka S, & Hirokawa N (1998). Golgi vesiculation and lysosome dispersion in cells lacking cytoplasmic dynein. Journal of Cell Biology, 141, 51–59.

Hatch EM & Hetzer MW (2016). Nuclear envelope rupture is induced by actin-based nucleus confinement. Journal of Cell Biology, 215, 27–36.

Heimann K, Percival JM, Weinberger R, Gunning P, & Stow JL (1999). Specific isoforms of actin-binding proteins on distinct populations of Golgi-derived vesicles. Journal of Biological Chemistry, 274, 10743–10750.

Heissler SM & Sellers JR (2016). Kinetic adaptations of myosins for their diverse cellular functions. Traffic, 17, 839–859. [PubMed: 26929436]

Hsu RM, Tsai MH, Hsieh YJ, Lyu PC, & Yu JS (2010). Identification of MYO18A as a novel interacting partner of the PAK2/beta-PIX/GIT1 complex and its potential function in modulating epithelial cell migration. Molecular Biology of the Cell, 21, 287–301. [PubMed: 19923322]

Jacob R, Heine M, Alfalah M, & Naim HY (2003). Distinct cytos-keletal tracks direct individual vesicle populations to the apical membrane of epithelial cells. Current Biology, 13, 607–612. [PubMed: 12676094]

Kengyel A, Wolf WA, Chisholm RL, & Sellers JR (2010). Non-muscle myosin IIA with a GFP fused to the N-terminus of the regulatory light chain is regulated normally. Journal Muscle Research & Cell Motility, 31, 163–170.

Kepes F, Rambourg A, & Satiat-Jeunemaitre B (2005). Morphodynamics of the secretory pathway. International Review of Cytology, 242, 55–120. [PubMed: 15598467]

Khatau SB, Hale CM, Stewart-Hutchinson PJ, Patel MS, Stewart CL, Searson PC, … Wirtz D (2009). A perinuclear actin cap regulates nuclear shape. Proceedings of the National Academy of Science of United States of America, 106, 19017–19022.

Kim DH, Khatau SB, Feng Y, Walcott S, Sun SX, Longmore GD, Wirtz D 2012. Actin cap associated focal adhesions and their distinct role in cellular mechanosensing. Scientific Reports, 2, 555. [PubMed: 22870384]

Kirkbride KC, Hong NH, French CL, Clark ES, Jerome WG, & Weaver AM (2012). Regulation of late endosomal/lysosomal maturation and trafficking by cortactin affects Golgi morphology. Cytoskeleton (Hoboken), 69, 625–643. [PubMed: 22991200]

Lazaro-Dieguez F, Colonna C, Cortegano M, Calvo M, Martinez SE, & Egea G (2007). Variable actin dynamics requirement for the exit of different cargo from the trans-Golgi network. FEBS Letters, 581, 3875–3881. [PubMed: 17651738]

Matas OB, Martinez-Menarguez JA, & Egea G (2004). Association of Cdc42/N-WASP/Arp2/3 signaling pathway with Golgi membranes. Traffic, 5, 838–846. [PubMed: 15479449]

Miller PM, Folkmann AW, Maia AR, Efimova N, Efimov A, & Kaverina I (2009). Golgi-derived CLASP-dependent microtubules control Golgi organization and polarized trafficking in motile cells. Nature Cell Biology, 11, 1069–1080. [PubMed: 19701196]

Minin AA (1997). Dispersal of Golgi apparatus in nocodazole-treated fibroblasts is a kinesin-driven process. Journal of Cell Science, 110, 2495–2505. [PubMed: 9410887]

Miserey-Lenkei S, Chalancon G, Bardin S, Formstecher E, Goud B, & Echard A (2010). Rab and actomyosin-dependent fission of transport vesicles at the Golgi complex. Nature Cell Biology, 12, 645–654. [PubMed: 20562865]

Mori K, Furusawa T, Okubo T, Inoue T, Ikawa S, Yanai N, … Obinata M (2003). Genome structure and differential expression of two isoforms of a novel PDZ-containing myosin (MysPDZ) (Myo18A). Journal of Biochemistry, 133, 405–413. [PubMed: 12761286]

Author Manuscript Author Manuscript Author Manuscript Author Manuscript

Mori K, Matsuda K, Furusawa T, Kawata M, Inoue T, & Obinata M (2005). Subcellular localization and dynamics of MysPDZ (Myo18A) in live mammalian cells. Biochemical & Biophysical Research Communications. 326, 491–498. [PubMed: 15582604]

Palade G (1975). Intracellular aspects of the process of protein synthesis. Science, 189, 347–358. [PubMed: 1096303]

Ran FA, Hsu PD, Wright J, Agarwala V, Scott DA, & Zhang F (2013). Genome engineering using the CRISPR-Cas9 system. Nature Protocols, 8, 2281–2308. [PubMed: 24157548]

Sanders AA & Kaverina I (2015). Nucleation and dynamics of golgi-derived microtubules. Frontiers in Neuroscience, 9, 431. [PubMed: 26617483]

Stow JL, Fath KR, & Burgess DR (1998). Budding roles for myosin II on the Golgi. Trends in Cell Biology, 8, 138–141. [PubMed: 9695826]

Taft MH, Behrmann E, Munske-Weidemann LC, Thiel C, Raunser S, & Manstein DJ (2013). Functional characterization of human myosin-18A and its interaction with F-actin and GOLPH3. Journal of Biological Chemistry, 288, 30029–30041.

Tan I, Yong J, Dong JM, Lim L, & Leung T (2008). A tripartite complex containing MRCK modulates lamellar actomyosin retrograde flow. Cell, 135, 123–136. [PubMed: 18854160]

Thyberg J & Moskalewski S (1999). Role of microtubules in the organization of the Golgi complex. Experimental Cell Research, 246, 263–279. [PubMed: 9925741]

Valderrama F, Babia T, Ayala I, Kok JW, Renau-Piqueras J, & Egea G (1998). Actin microfilaments are essential for the cytological positioning and morphology of the Golgi complex. European Journal of Cell Biology, 76, 9–17. [PubMed: 9650778]

Vinogradova T, Paul R, Grimaldi AD, Loncarek J, Miller PM, Yampolsky D, … Kaverina I (2012). Concerted effort of centrosomal and Golgi-derived microtubules is required for proper Golgi complex assembly but not for maintenance. Molecular Biology of the Cell, 23, 820–833. [PubMed: 22262454]

Vishavkarma R, Raghavan S, Kuyyamudi C, Majumder A, Dhawan J, & Pullarkat PA (2014). Role of actin filaments in correlating nuclear shape and cell spreading. PLoS One, 9, e107895. [PubMed: 25251154]

Wang F, Kovacs M, Hu A, Limouze J, Harvey EV, & Sellers JR (2003). Kinetic mechanism of non-muscle myosin IIB: Functional adaptations for tension generation and maintenance. Journal of Biological Chemistry, 278, 27439–27448.

Yadav S, Puthenveedu MA, & Linstedt AD (2012). Golgin160 recruits the dynein motor to position the Golgi apparatus. Developmental Cell, 23, 153–165. [PubMed: 22814606]

Zhu X & Kaverina I (2013). Golgi as an MTOC: Making microtubules for its own good. Histochemistry & Cell Biology, 140, 361–367. [PubMed: 23821162]

Author Manuscript Author Manuscript Author Manuscript Author Manuscript

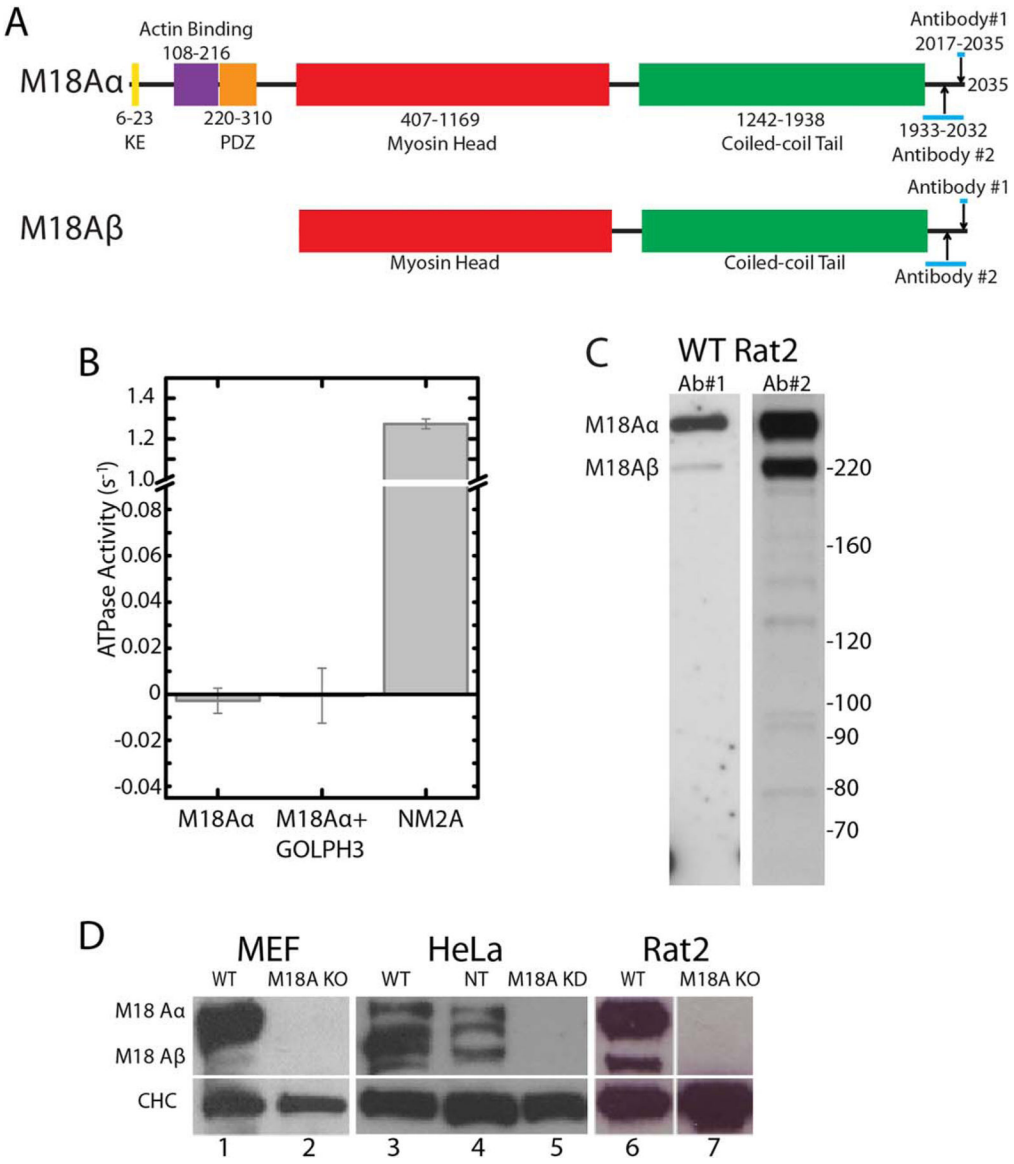

FIGURE 1.

M18A domain organization, actin-activated ATPase activity, antibody specificity, and knockdown/knockout cell lines (a) Domain organization of M18Aα and M18Aβ with amino acid numbers indicated. Relative to M18Aβ, M18Aα possesses a ~332 residue N-terminal extension that contains a lysine/glutamate (KE)-rich domain (yellow), an actin binding domain (purple), and a PDZ domain (orange). The regions of sequence used to generate Antibodies #1 and #2, which are identical in both isoforms, are shown in blue. (b) Actin-activated ATPase activities of purified M18Aα in the presence and absence of purified GOLPH3, and of NM2A (see Methods for details). (c) Western blot of a Rat2 whole cell extract probed with Antibody #1 (left lane) and Antibody #2 (right lane). Molecular weight markers are shown on the right in kDa. Both antibodies specifically recognize M18Aα and M18Aβ. (d) Western blots of extracts from the indicated cell types probed with Antibody #1 (WT stands for wild-type, NT stands for nontargeting shRNA). The positions of M18Aα

and M18Aβ are indicated. The bottom panels show the loading control (anti-clathrin heavy chain; CHC). See also Figure S1 in Supporting Information [Color figure can be viewed at wileyonlinelibrary.com]

Author Manuscript Author Manuscript Author Manuscript Author Manuscript

Author Manuscript Author Manuscript Author Manuscript Author Manuscript

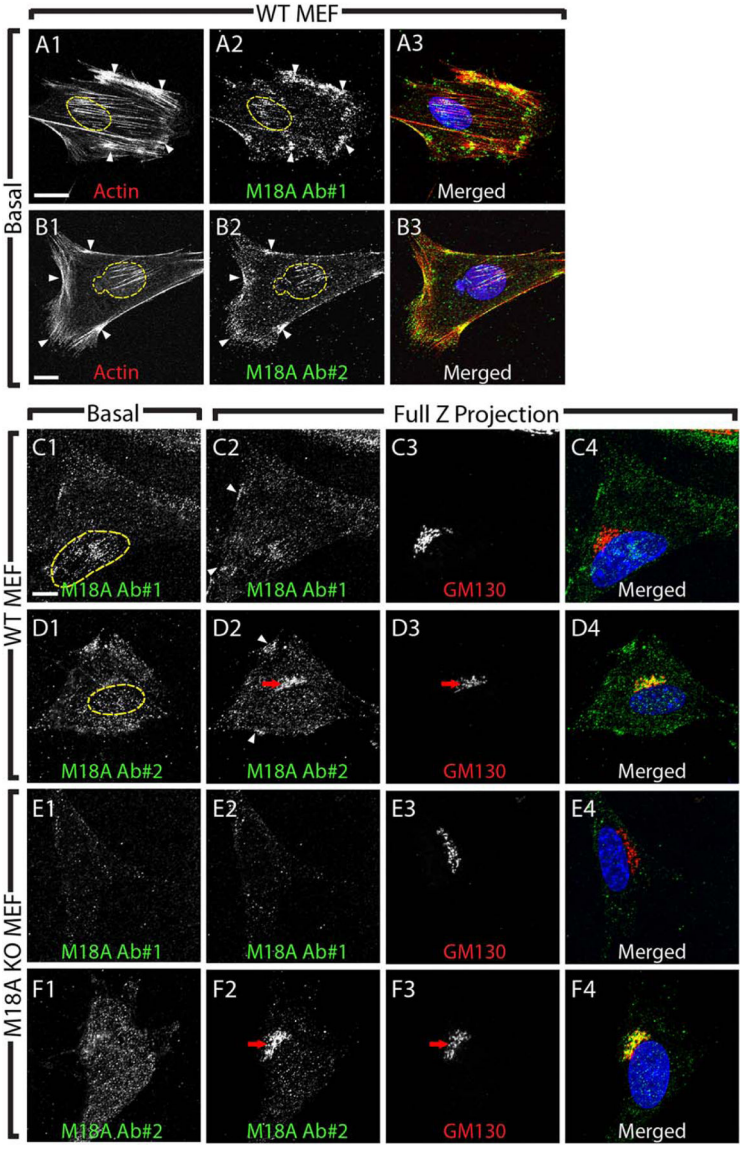

FIGURE 2.

Endogenous M18Aα does not localize to the Golgi. (a) Wild-type (WT) MEF fixed and stained for F-actin (phalloidin, a1) and M18A (Antibody #1, a2). The merged image in (a3) includes the signal for the nucleus (DAPI, blue). The position of the nucleus is marked with a yellow dashed line in (a1 and a2). White arrowheads mark cortical regions where M18A and actin are enriched. The images are maximum intensity projections of the bottom five 0.236 μm slices from a z-stack acquired on a Nikon A1R confocal microscope ("Basal"). Scale bar, 20 μm. (b) Exactly as in (a) except using Antibody #2. (c) WT MEF fixed and stained for M18A (Antibody #1, c1 and c2) and the Golgi (GM130, c3). The merged image in (c4) includes the signal for the nucleus (DAPI, blue). The position of the nucleus is marked with a yellow dashed line in (c1). White arrowheads in (c2) mark cortical regions where M18A and actin are enriched. (c1) is a maximum intensity projection of the bottom five 0.236 μm slices from the full z-stack ("Basal"). (c2–c4) are maximum intensity

Author Manuscript Author Manuscript Author Manuscript Author Manuscript

projections of all 0.236 μm slices acquired on a Nikon A1R confocal microscope ("Full Z Projection"). Scale bar, 10 μm. (d) Exactly as in (c) except using Antibody #2. The apparent co-localization between M18A and the Golgi is marked with red arrows. (e and f) Exactly as in (c and d) except using a M18A KO MEF. Note that the apparent colocalization between M18A and the Golgi (red arrows) seen with Antibody #2 in (d) persists in cells lacking M18Aα and M18Aβ in (f) [Color figure can be viewed at wileyonlinelibrary.com]

Author Manuscript Author Manuscript Author Manuscript Author Manuscript

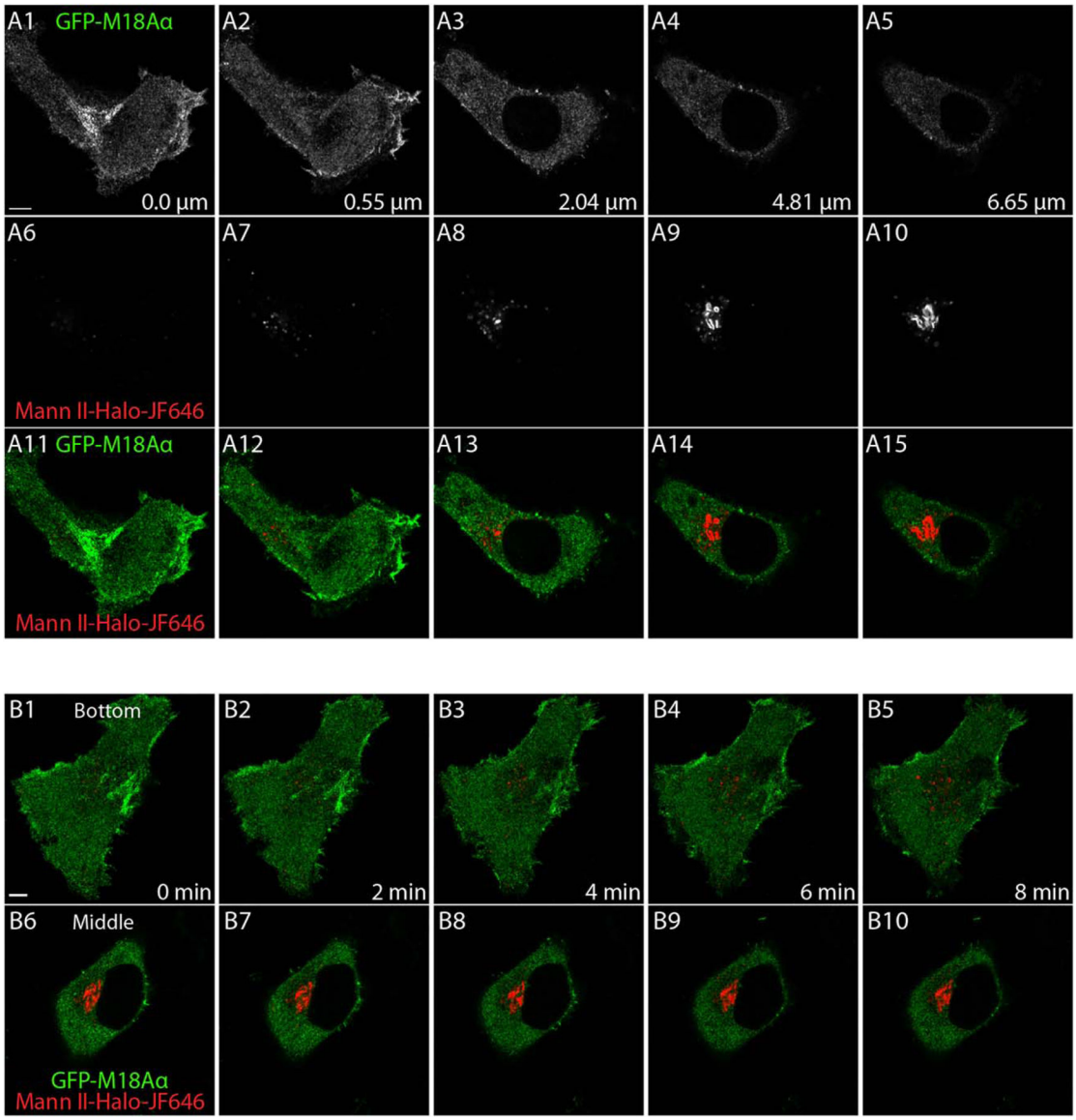

FIGURE 3.

GFP-tagged M18Aα does not localize to the Golgi. (a) HeLa cell expressing EGFP-M18Aα (green) and Mann II-Halo-646 (red) were imaged using a Zeiss Airyscan microscope. Selected optical sections from a complete z-stack are shown from left to right in increasing distance from the cell bottom (distance from the cell bottom indicated in lower right corner of a1–a5). (a1–a5) show M18Aα localization, (a6–a10) show Golgi localization, and (a11–a15) show the merged images. Scale bar, 5 µm. (b) HeLa cell prepared as in (a) was imaged over 8 min in just two planes: at the bottom (b1–b5) and in the middle (3.7 µm above the coverslip) of the cell (b6–b10), and all the panels are merged images of the M18Aα (green) and Golgi (red) at the indicated time points. See also Video S1 in Supporting Information [Color figure can be viewed at wileyonlinelibrary.com]

Author Manuscript Author Manuscript Author Manuscript Author Manuscript

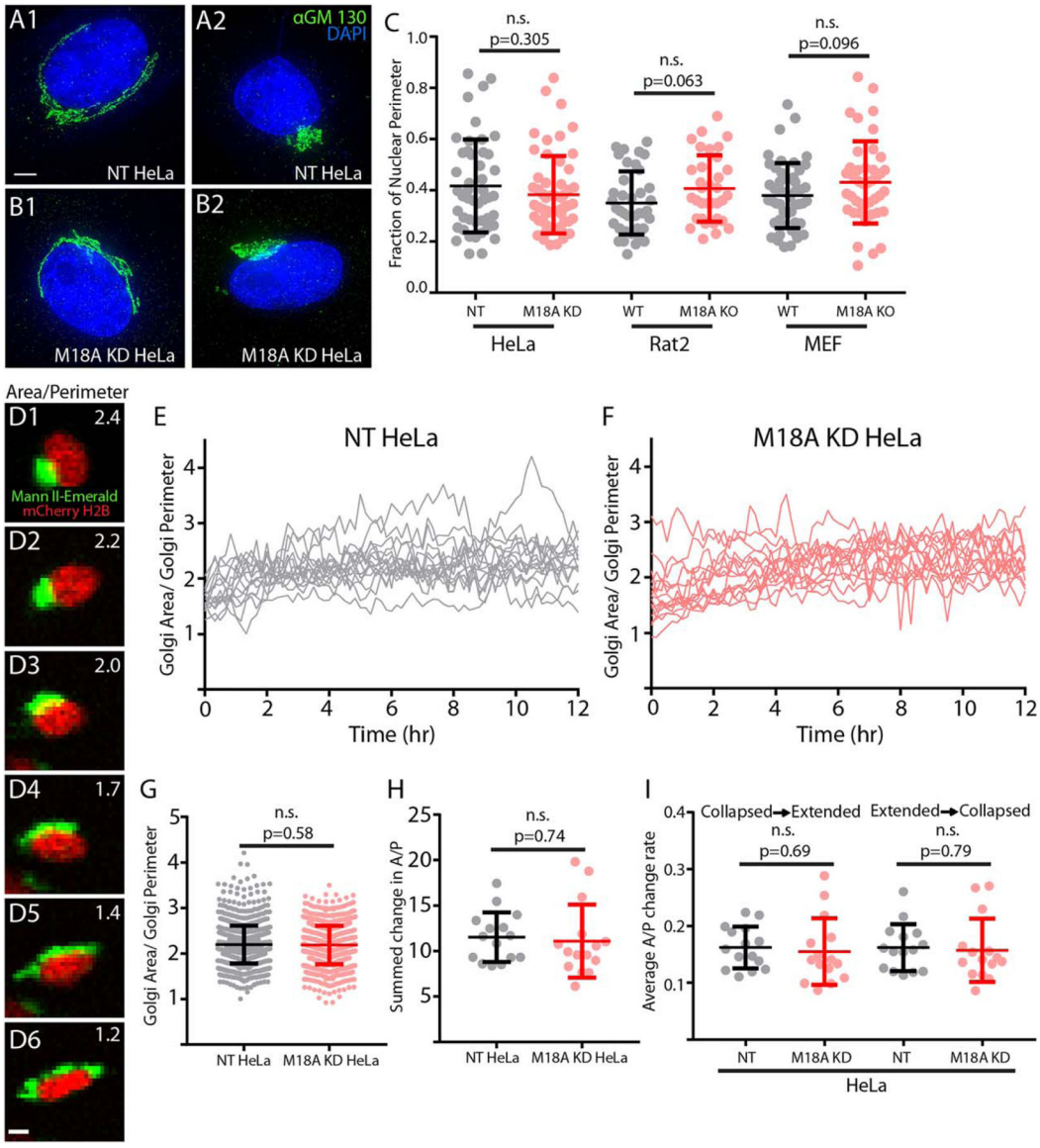

FIGURE 4.

Abrogation of M18Aα expression does not alter Golgi morphology, which is highly variable. (a and b) Control HeLa cells expressing non-targeting (NT) shRNA (NT HeLa, a1 and a2) and Hela cells expressing M18A shRNA (M18A KD HeLa, b1 and b2) were fixed and stained with the cis-Golgi marker α-GM130 (green) and the nuclear marker DAPI (blue). The images are maximum intensity projections of wide-field z-stacks acquired on a Deltavision OMX microscope with 0.125 μm steps. These representative images show that the Golgi can exist in both extended and contracted states in both control and M18A KD cells. Scale bar, 5 μm. (c) Golgi size, quantified as a fraction of nuclear perimeter, was measured in the indicated cell types prepared and was imaged as in (a) and (b). The n values are as follows: NT HeLa (47), M18A KD HeLa (55), WT Rat2 (39), M18A KO Rat2 (49), WT MEF (49), and M18A KO MEF (43). (d) NT HeLa cell expressing mCherry-H2B to mark the nucleus (red) and Mann II-mEmerald to mark the Golgi (green) and was imaged

Author Manuscript Author Manuscript Author Manuscript Author Manuscript

using a Nikon A1R microscope. Shown are representative examples of the variations in Golgi morphology exhibited by this cell over time (*A/P* values are shown in the upper right corner). Scale bar, 10 μm. (e) *A/P* values for 15 randomly chosen NT HeLa cells (grey) imaged as described in (d) every 10 min over 12 hr. (f) Exactly as in (e) but with M18A KD HeLa cells (red). (g) Means and standard deviations for all the *A/P* values obtained over 12 hr for NT HeLa (grey) and M18A KD HeLa (red). (H) Means and standard deviations for the summed changes in *A/P* values over 12 hr for NT HeLa (grey) and M18A KD HeLa (red). (i) Means and standard deviations for the rates of change in *A/P* values per 10-min interval going from either collapsed to extended and or from extended to collapsed for NT HeLa (grey) and M18A KD HeLa (red). Where appropriate, p values are indicated (n.s. indicates a lack of significance) [Color figure can be viewed at wileyonlinelibrary.com]

Author Manuscript Author Manuscript Author Manuscript Author Manuscript

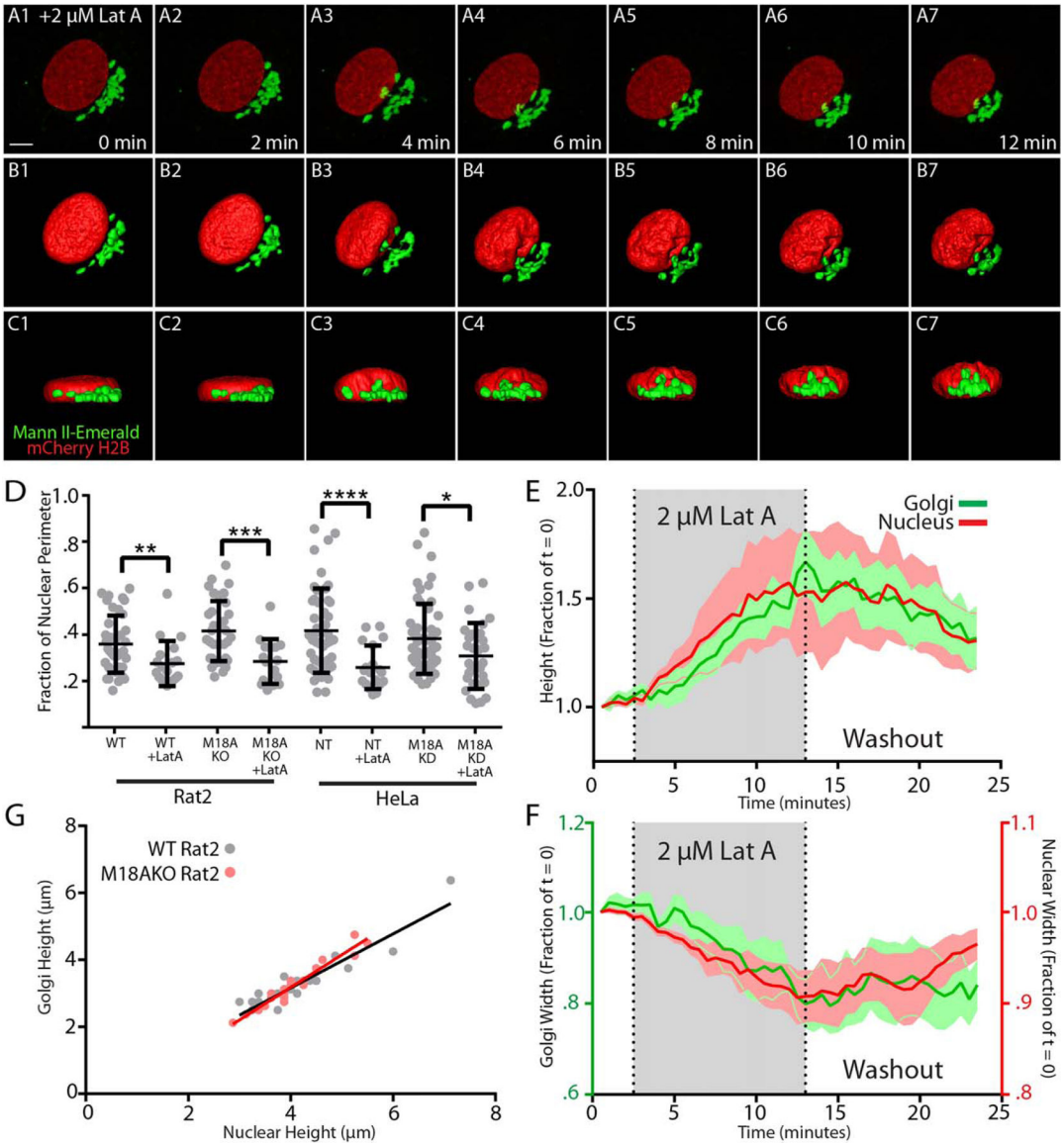

FIGURE 5.

Actin filament disassembly causes changes in Golgi morphology that correlate with changes in nuclear shape. (a–c) A Rat2 cell expressing mCherry-H2B to mark the nucleus (red) and Mann II-mEmerald to mark the Golgi (green) was imaged in 0.5 µm steps on a Zeiss Airyscan microscope every 2-min following addition of 2 µM Lat A (time indicated in lower right corner of a1–a7). Shown are maximum intensity projections from an overhead view (a1–a7), 3D surface-rendered images from an overhead view (b1–b7), and 3D surface-rendered images from an orthogonal view (c1–c7). Scale bar, 5 µm. Note in panels (c1–c7) that as the Golgi undergoes a reduction in width, it increases in height, and that the nucleus undergoes a similar reduction in width and increase in height. See also Video S3 in Supporting Information. (d) Golgi size, quantified as a fraction of nuclear perimeter, measured in the indicated cell types either before or 15 min after addition of 2 µM Lat A, and following fixation and staining with α-GM130 and DAPI. Lines indicate mean +/−

Author Manuscript Author Manuscript Author Manuscript Author Manuscript

standard deviation. The p values are as follows: WT Rat2 vs. WT Rat2 + Lat A, $p = 0.0073$; M18A KO Rat2 vs. M18A KO Rat2 + Lat A, $p = 0.0003$; NT HeLa vs. NT HeLa + Lat A, $p < 0.0001$; M18A KD HeLa vs. M18A KD HeLa + Lat A, $p = 0.0295$. The n values are as follows: WT Rat2 (39), WT Rat2 + Lat A (19), M18A KO Rat2 (34), M18A KO Rat2 + Lat A (16), NT HeLa (47), NT HeLa + Lat A (19), M18A KD HeLa (55), M18A KO HeLa + Lat A (29). (e and f) Eight Rat2 cells expressing Mann II-mEmerald and mCherry-H2B were imaged for 2.5 min prior to Lat A addition, for 10 min in the presence of 2 μM Lat A (grey background), and for 12.5 min after Lat A washout (white background). Panel (e) shows the heights of Golgi (green) and nuclei (red), plotted as fractions of $t = 0$, while Panel (f) shows the widths of Golgi (green) and nuclei (red), plotted as fractions of $t = 0$. In both panels, the mean values are indicated by the dark red and green lines, while the SEM values are indicated by the light red and green shaded areas. Note that the scales for Golgi and nuclei in Panel (f) are different. The changes in nuclear and Golgi shape are significantly correlated in both height ($R^2 = 0.88$, $p \leq 0.0001$) and width ($R^2 = 0.72$, $p \leq 0.0001$). (g) WT Rat2 cells (grey) and M18A KO Rat2 cells (red) were fixed and stained with the cis-Golgi marker α-GM130 (green) and the nuclear marker DAPI (blue), and the heights of their nuclei (x axis) and Golgi (y axis) measured ($n = 23$). Linear regression analyses demonstrated a strong positive correlation between Golgi height and nuclear height for both WT ($R^2 = 0.86$; slope = 0.81) and M18A KO cells ($R^2 = 0.94$; slope = 0.97), and slopes that are significantly nonzero ($p \leq 0.0001$) [Color figure can be viewed at wileyonlinelibrary.com]

Author Manuscript Author Manuscript Author Manuscript Author Manuscript

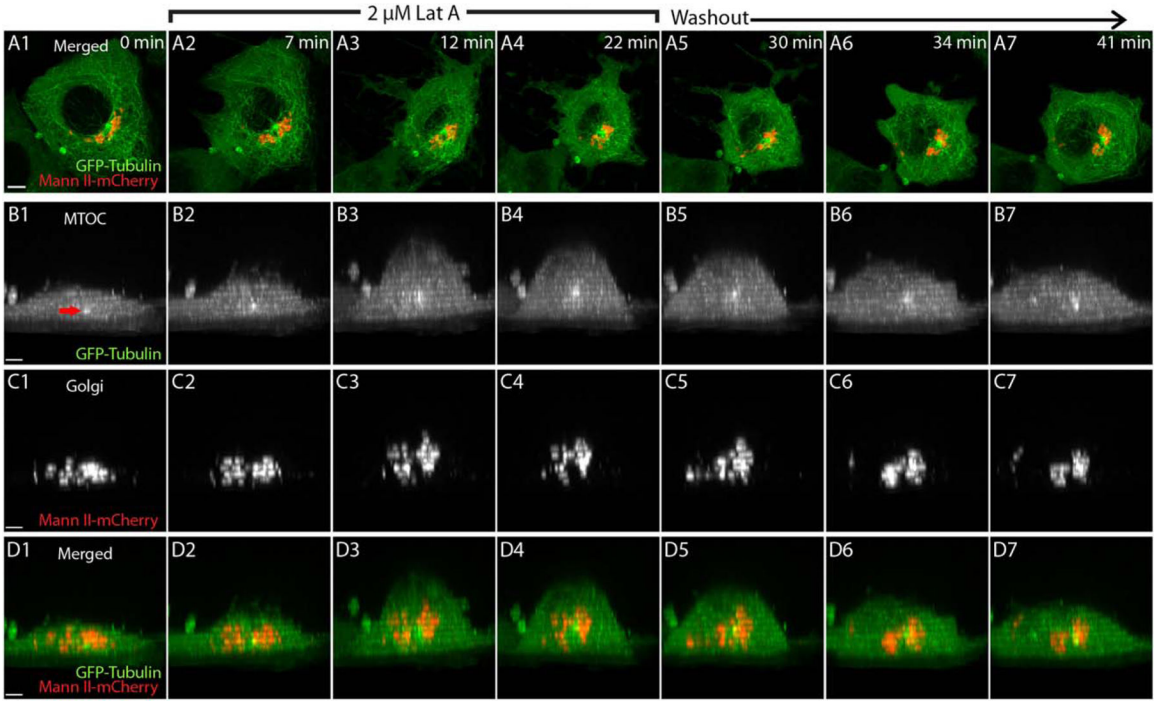

FIGURE 6.

Actin filament disassembly induces vertical movement of the MTOC that parallels the increase in Golgi height. (a–d) A Rat2 cell expressing GFP-tubulin to mark the MTOC (the single, bright, perinuclear green spot marked with a red arrow in Panel b1) and Mann II-mCherry to mark the Golgi (red) was imaged in 1 μm steps on a Zeiss Airyscan microscope at the indicated time points (upper right corner in a1–a7) before, during, and after treatment with 2 μM Lat A, as indicated. Shown are maximum intensity projections for the merged images from an overhead view (a1-a7), and maximum intensity projections for the MTOC (b1-b7, see arrowhead), Golgi (c1-c7), and merged (d1-d7) from orthogonal views. See also Video S4 in Supporting Information. The horizontal striping apparent in the orthogonal views stems from the suboptimal axial sampling required to execute super-resolution imaging and can be ignored. Scale bars, 4 μm in (a) and 3 μm in (b–d) [Color figure can be viewed at wileyonlinelibrary.com]